Title: Precipitable water and CAPE dependence of rainfall intensities in China

Authors: Wenhao Dong[1], Yanluan Lin[1], Jonathon S. Wright[1], Yuanyu Xie[1], Xungang Yin[2], Jianping Guo[3]

[1]Ministry of Education Key Laboratory for Earth System Modeling, Department of Earth System Science, and Joint Center for Global Change Studies (JCGCS), Tsinghua University, Beijing 100084, China.
[2]ERT, Inc., at NOAA National Climatic Data Center, Asheville, NC 28801, USA
[3]State Key Laboratory of Severe Weather and Key Laboratory of Atmospheric Chemistry of China Meteorological Administration (CMA), Chinese Academy of Meteorological Sciences, Beijing 100081, China.

Corresponding author: Yanluan Lin
Email: yanluan@tsinghua.edu.cn, Tel: +1186 (10) 6279-7763

Abstract
The influence of temperature on precipitation in China is investigated from two aspects of the atmospheric water cycle: available water vapor and atmospheric instability. Daily observations are used to analyze how rainfall intensities and its spatial distribution in mainland China depend on these two aspects. The results show that rainfall intensities, and especially rainfall extremes, increase exponentially with available water vapor. The efficiency of water vapor conversion to rainfall is higher in northwestern China where water vapor is scarce than in southeastern China where water vapor is plentiful. The results also reveal a power law relationship between rainfall intensity and convective instability. The fraction of convective available potential energy (CAPE) converted to upward velocity is much larger over southeastern China than over the arid northwest. The sensitivities of precipitation to temperature-induced changes in available water vapor and atmospheric convection are thus geographically reciprocal. Specifically, while conversion of water vapor to rainfall is relatively less efficient in southeastern China, conversion of CAPE to upward kinetic energy is more efficient. By contrast, in northwestern China, water vapor is efficiently converted to rainfall but only a small fraction of CAPE is converted to upward motion. The detailed features of these relationships vary by location and season; however, the influences of atmospheric temperature on rainfall intensities and rainfall extremes are predominantly expressed through changes in available water vapor, with changes in convective instability playing a secondary role.

Keywords: convective instability; available water vapor; rainfall intensity; China

1. Introduction

Relationships between atmospheric temperature and precipitation intensity are of great concern for human society, particularly as climatic warming intensifies the hydrologic cycle (Allen and Ingram, 2002; Wang and Zhou, 2005; Trenberth, 2011; Donat *et al.*, 2016). Previous studies have helped to constrain these relationships on a variety of time scales (Held and Soden, 2006; Allan and Soden, 2008; O'Gorman and Schneider, 2009; Utsumi *et al.*, 2011; Berg *et al.*, 2009), but several aspects of the results remain controversial. This lack of consensus is fueled in part by large seasonal and regional variations in the temperature dependence of rainfall (Berg *et al.*, 2009; Hardwick Jones *et al.*, 2010; Utsumi *et al.*, 2011).

The dependence of rainfall on temperatures has been explored from a variety of perspectives (Allen and Ingram, 2002; Trenberth *et al.*, 2003; Haerter and Berg, 2009; Lepore *et al.*, 2015). Many of these studies have focused on changes in the water vapor saturation capacity of the atmosphere, which depends on tropospheric temperature via the Clausius-Clapeyron relation. Increases in saturation capacity due to increasing tropospheric temperatures lead to enhanced rainfall, provided that the enhanced moisture eventually returns to the surface (Trenberth *et al.*, 2003; Donat *et al.*, 2016). Rainfall intensity and extreme rainfall may also be controlled by variations in atmospheric convection, particularly when precipitation is dominated by local surface forcing (Trenberth and Shea, 2005; Adams and Souza, 2009; Lepore *et al.*, 2015). Increases in convective instability under a warming climate may lead to an increase in the proportion of convective rainfall, which could be modulated by changes in environmental conditions, such as the moist adiabatic temperature lapse rate, or changes in the average characteristics of convection, such as updraft velocities (Allen and Ingram, 2002; Haerter and Berg, 2009; O'Gorman and Schneider, 2009; Singh and O'Gorman, 2013; Brooks *et al.*, 2014). Thus, the roles of atmospheric moisture content and convective properties should both be taken into consideration when evaluating the response of rainfall to temperature variations.

Despite projections that the number of extreme precipitation events will increase under global warming (Yuan *et al.*, 2015), few studies to date have investigated how these two factors influence rainfall intensities in China. Here we investigate the dependence of rainfall intensity on available moisture and convective instability using daily observations from a large number of meteorological stations in mainland China. The role of available moisture is evaluated using precipitable water (PW), while that of convective instability is evaluated using convective available potential energy (CAPE). PW measures the integrated water content in a column of the atmosphere, such that a higher value of PW indicates a larger amount of available moisture. CAPE is an energy-based measure of atmospheric potential instability that has been widely used to infer key characteristics of convective instability (Brooks *et al.*, 1994; Lepore *et al.,* 2015). This metric defines the theoretical maximum velocity that a positively buoyant air parcel could acquire through adiabatic ascent (DeMott and Randall, 2004; North and Erukhimova, 2009; Lepore *et al.*, 2015). Larger values of CAPE thus indicate greater potential for strong updrafts in convective storms.

The data and methods used in this work are described in Section 2. Key results, including the climatology and seasonal distributions of precipitation, PW, and CAPE and the dependence of precipitation intensity on PW, CAPE, and their combination are presented in Section 3. Our conclusions are summarized in Section 4.

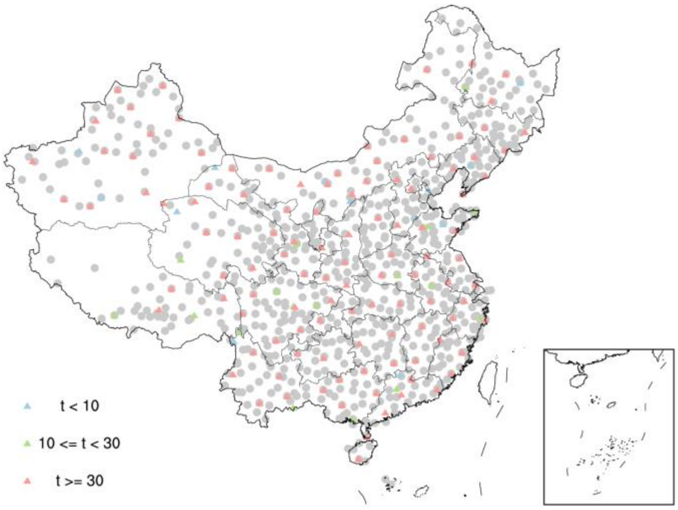

Figure 1. Station locations and types. Gray dots represent CMA stations that provide rainfall observations. Colored triangles represent radiosonde stations, with different colors corresponding to different observation spans (in years) as indicated by the key.

2. Data and methodology

2.1 Data sources

Daily precipitation data are provided by the China Meteorological Administration (CMA). These data were collected at 756 stations (Fig. 1; gray dots) during 1961–2014. The stations are maintained according to standards set by the CMA, which follow both the WMO Guide to the Global Observing System and CMA Technical Regulations on Weather Observations. We exclude snowfall records in this study considering the large uncertainties associated with snow observation.

PW and CAPE are derived from twice-daily (00 and 12 UTC) radiosonde profiles taken from version 2 of the Integrated Global Radiosonde Archive (IGRA; Durre, *et al.*, 2006; Durre, *et al.*, 2009). IGRA is the most comprehensive and largest international radiosonde data set compiled to date, and includes 144 stations in China (Fig. 1; colored triangles). The earliest observations in China date back to the late 1930s, with nearly 80% (111) of the 144 radiosonde stations providing observations over 30 years or more. The high temporal resolution, long record, and broad spatial sampling provided by IGRA are essential to the success of this study.

2.2 Methods

Values of PW are derived from radiosonde profiles on pressure levels according to the equation

$$PW = \frac{1}{g_0}\int_{500}^{SRF} \mathrm{q}\,dp$$

where g_0 is the average gravitational acceleration at Earth's surface, q is the specific humidity, and p is pressure. PW is defined as the integrated water vapor content of the atmosphere below the 500 hPa isobaric surface. This choice reflects the fact that water vapor resides mainly at lower levels of the atmosphere, where temperatures are relatively warm. Values of CAPE are derived from the same profiles according to the equation

$$CAPE = R_d \int_{LFC}^{LNB} (\mathrm{T}_p - \mathrm{T}_e) d \ln p$$

where R_d is the gas constant for dry air, T_p is the parcel temperature along a moist adiabat, and T_e is the environment temperature from the radiosonde profile. CAPE is conventionally defined as the integral of the positive portion of the parcel buoyancy between the level of free convection (LFC) and the level of neutral buoyancy (LNB). The effect of water vapor on the parcel buoyancy (the “virtual temperature correction”; Doswell and Rasmussen, 1994; Emanuel, 1994) was excluded here to better differentiate variations in available water from variations in convective instability. Twice-daily values are averaged to daily means for the analysis to reduce diurnal sampling biases associated with the large east−west span of China (PW and CAPE are recorded at regular intervals in Coordinated Universal Time).

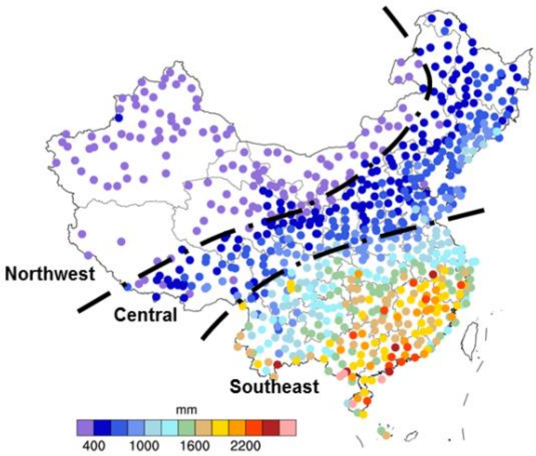

Figure 2. Distribution of annual total precipitation from 756 CMA stations. We use this distribution to divide mainland China into three sub-regions: southeastern China (where annual precipitation is typically greater than ~1000 mm), central China (where annual precipitation is typically between 400~1000 mm), and northwestern China (where annual precipitation is typically less than ~400 mm).

We pair each radiosonde station with its nearest neighbor among the CMA precipitation stations. Any station pair covering less than 10 years is excluded from the analysis, yielding 127 pairs of stations. To account for large precipitation gradients across mainland China, we partition the analysis domain into three sub-regions corresponding to southeastern China, central China and northwestern China (Fig. 2) and pool the data within each subset. The classification is determined such that each sub-region has a unique regional rainfall regime and a reasonable number of stations. The number of paired stations in each sub-region is 43 (southeast), 42 (central), and 42 (northwest), indicating a relatively homogenous and representative distribution. This procedure ensures consistent sample sizes and robust statistical comparisons among the three sub-regions.

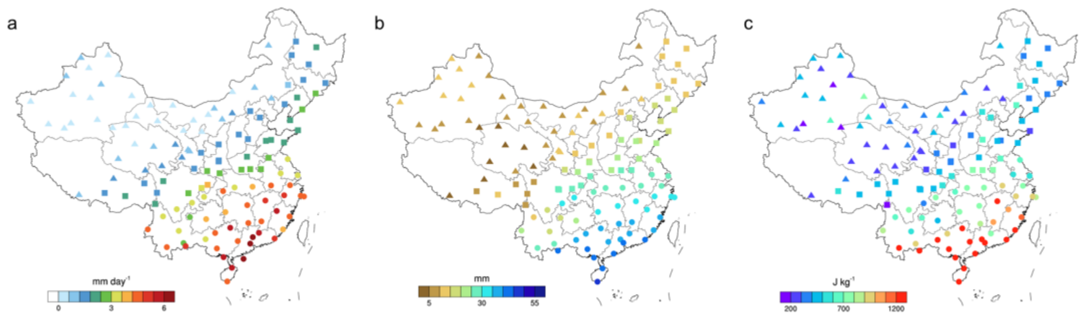

Figure 3. Climatological distributions of (a) precipitation, (b) PW, and (c) CAPE for 127 pairs of stations over mainland China. Solid dots, boxes, and triangles in a–c indicate stations located in the southeastern, central, and northwestern sub-regions, respectively (see Fig. 2 and text for details).

3 Results

3.1 Climatologies and seasonalities of precipitation, PW, and CAPE

Figure 3 shows geographical distributions of long-term mean daily precipitation, PW, and CAPE in mainland China during 1961–2014. Intermittent instrument failures mean that some radiosonde data are missing from the observation record, especially during the earlier stages and winter months. To avoid biased results towards to summertime values due to the sampling issue, we therefore calculate long-term means for each day of the year individually before averaging to get climatological and seasonal distributions. This approach allows us to construct representative climatologies using the maximum amount of available data. All three variables share a common southeast–northwest geographical gradient. Larger precipitation amounts are associated with larger values of PW and CAPE in southeastern China, while smaller precipitation amounts are associated with smaller values of PW and CAPE in northwestern China. For instance, values of cumulative annual precipitation decrease from more than 2000 mm in the southeast to less than 400 mm in the northwest (Fig. 2; Zhai *et al.*, 2005). Climatological mean values of PW (CAPE) similarly decline from more than 50 mm (1000 J kg^{-1}) to approximately 5 mm (200 J kg^{-1}). The partitioning separates China into three climatologically distinct sub-regions bounded by daily rainfall amounts of approximately 3 mm day^{-1} and 1 mm day^{-1}, respectively. These bounds roughly correspond to values of 30 mm and 15 mm in PW and values of 700 J kg^{-1} and 400 J kg^{-1} in CAPE (Fig. 3).

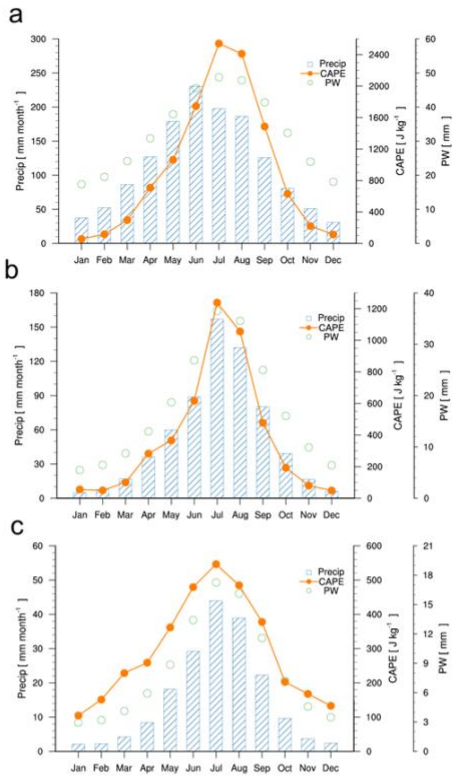

Figure 4. Seasonal cycles of precipitation (bars), PW (open circles), and CAPE (filled circles and solid lines) averaged over stations in (a) southeastern China (solid dots in Fig. 3), (b) central China (solid boxes in Fig. 3), and (c) northwestern China (solid triangles in Fig. 3). Note the different vertical scales in each panel.

Figure 4 shows typical seasonal evolutions of precipitation, PW, and CAPE for the three sub-regions. For each sub-region, all three variables follow well-defined seasonal cycles, with peak values during summer months (June-July-August) and minimum values during winter months (December-January-February). The seasonal cycle of precipitation is highly correlated with the seasonal cycles of PW and CAPE in each sub-region. All three regions show significant correlation coefficients (p<0.001) between the seasonal cycles of rainfall and PW, with r^2 equal to 0.86 (southeast), 0.98 (central), and 0.98 (northwest). Correlation coefficients between rainfall and CAPE are also strong and significant, with values of 0.77, 0.98, and 0.94, respectively. Maximum values of rainfall, CAPE, and PW in central and northwestern China occur in July (Fig. 4b–c). By contrast, maximum rainfall in southeastern China occurs in June, leading the maximum values of CAPE and PW by one month (Fig. 4a). This timing mismatch between peak rainfall and the peak values of convective instability and available moisture may be related to strong moisture convergence along the *Meiyu* front during the pre-monsoon period (Chen, 1994; Zhou and Li, 2002).

Comparing the months of monsoon onset (May) and withdrawal (September) in southeastern China, larger values of CAPE are observed in September than in May. This difference is in line with sea surface temperatures off the coast of southeastern China remaining warm for 1~2 months following the peak summer insolation, so that the ocean serves as a powerful source of heat and moisture to southeastern China during the autumn season. Situated far inland, oceanic influences on thermodynamic conditions in northwestern China are weak. The annual cycle of CAPE is thus more symmetric over northwestern China, with comparable values in May and September. By contrast, observed values of PW are larger in September than in May over central and northwestern China. This difference may reflect the "memory" of soil moisture following the infiltration of summer rainfall. Values of PW over southeastern China are more consistent in May and September due to the continuous supply of moisture from the surrounding oceans. These differences imply that PW may be more of a limiting factor for rainfall in arid northwestern China, while CAPE may be more of a limiting factor for rainfall in southeastern China. This hypothesis is explored in more detail below.

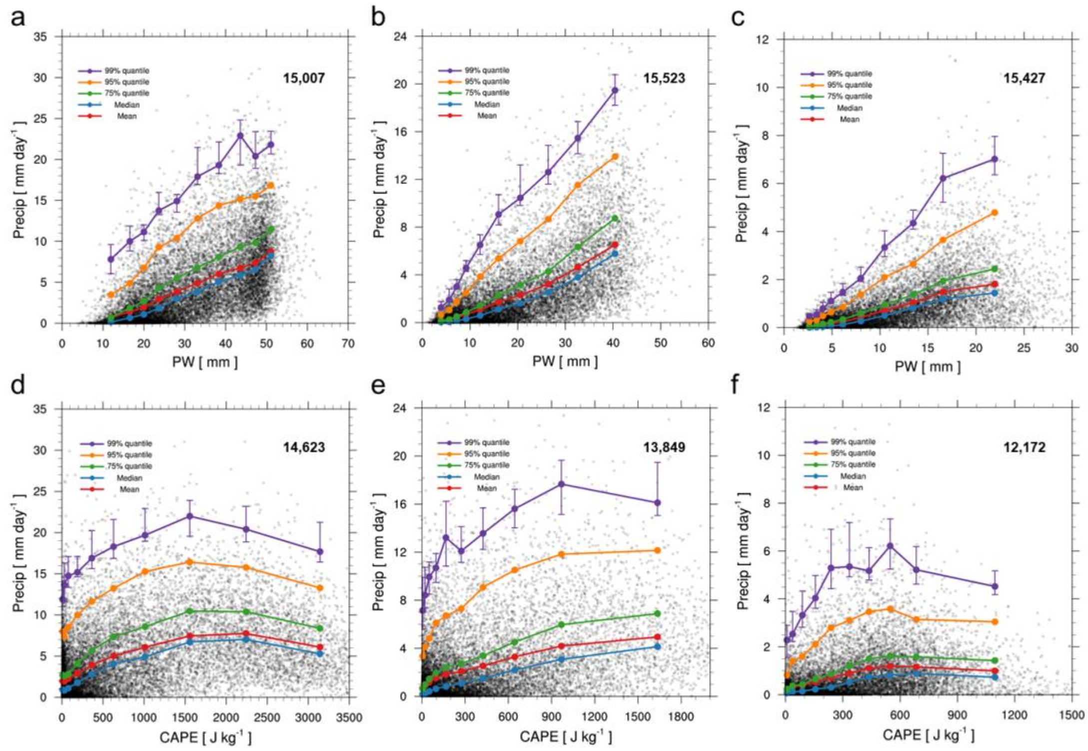

Figure 5. The mean dependence of rainfall on PW (a–c) and CAPE (d–f) averaged over southeastern China (a, d), central China (b, e), and northwestern China (c, f). Dots represent available events averaged over each sub-region. The number of samples in each sub-region is listed in the upper right quadrant of each panel. Error bars on the 99th percentile points indicate the 95% confidence level estimated using an interpolated order statistic approach. Note the different axis scales among the panels.

3.2 Dependence of precipitation on PW

Most observations are associated with lighter precipitation and smaller values of PW. We therefore bin the daily samples into ten intervals based on the deciles of PW. This approach ensures that each bin contains roughly the same number of samples, as opposed to intervals of equal width in PW. Our conclusions are qualitatively insensitive to the number of selected bins. For the following analysis, we extract several precipitation quantiles from each bin. Confidence intervals for quantiles are estimated based on the interpolated order statistic approach suggested by Hettmansperger and Sheather (1986) and Nyblom (1992).

We use two different methods to explore the dependence of rainfall on PW in each sub-region. In the first approach, we average all station records within the sub-region to identify the mean-state relationship between rainfall and PW (Fig. 5a–c). As expected, rainfall and PW have a positive relationship, with higher PW corresponding to larger precipitation (Ye *et al.*, 2014). This relationship is consistent throughout the three sub-regions, with the PW-dependence of each metric nearly linear across a wide range of precipitation intensities (mean precipitation and rainfall quantiles corresponding to the 50th, 75th, 95th, and 99th percentiles). These results indicate that, on average, rainfall intensity has a simple scaling relationship with PW. The slopes of all quantile lines are less than one for all three sub-regions. This is consistent with indications that lower-tropospheric moisture content increases faster than rainfall (Trenberth 1998; Held and Soden, 2006).

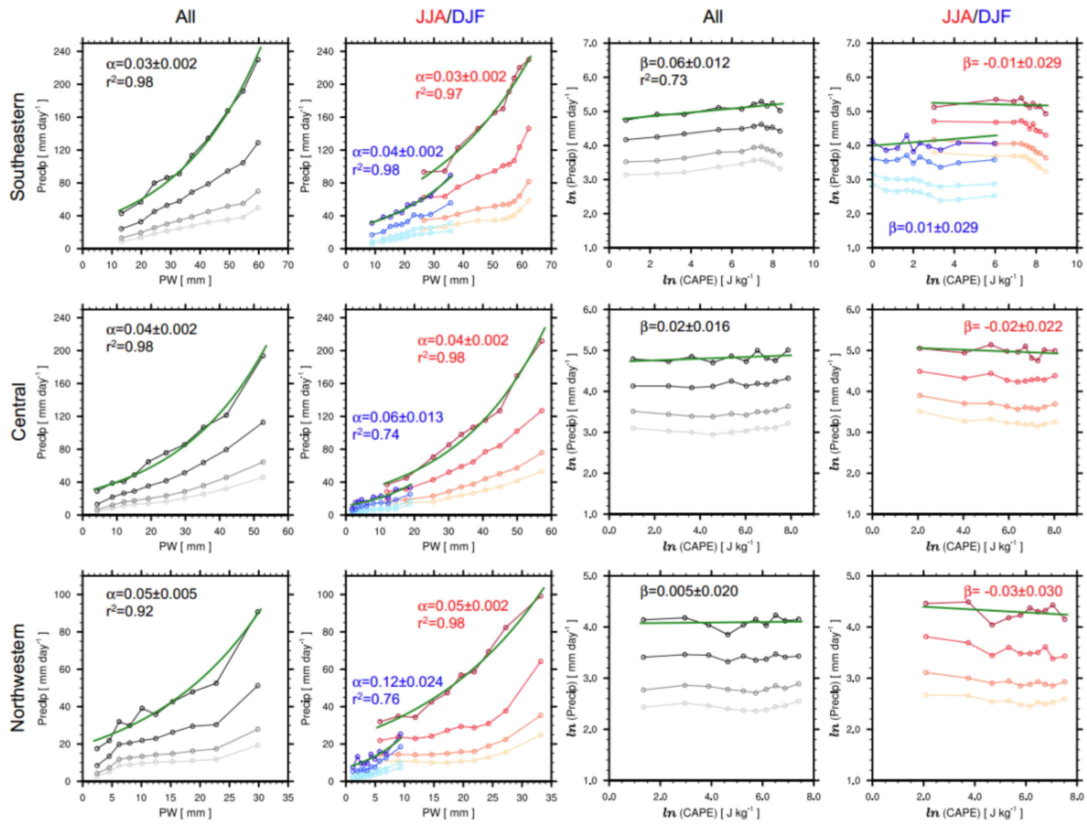

Figure 6. Dependence of extreme precipitation on PW (first and second columns) and CAPE (third and fourth columns) over southeastern China (upper panel), central China (middle panel), and northwestern China (bottom panel). The first and third columns show results for the entire calendar year. The second and fourth columns show results for the boreal winter (December-January-February, blue colors) and summer (June-July-August, red colors) solstice seasons. The green solid lines in the left two columns indicate exponential fit lines for the 99.9% precipitation quantiles. The green solid lines in the third and fourth columns indicate linear fit lines for the same 99.9% precipitation quantiles. For each plot, the intensity of the line color increases as the percentiles increase (p=0.9, 0.95, 0.99, and 0.999). Only results

for bins with sample sizes larger than 500 are shown. Fit coefficients (± one S.E.) are listed in each panel, with values of r^2 included when the fit is statistically significant.

This first approach gives an overall understanding of the dependence of rainfall on PW, but may average out the sensitivity of larger rainfall events, and especially rainfall extremes. The second approach takes all available rainfall events into consideration, focusing on four large precipitation quantiles (p=0.9, 0.95, 0.99, and 0.999). To explore the dependence of rainfall on PW in different seasons, conditional analyses are applied to events occurring during boreal summer (June-July-August) and winter (December-January-February). The results are displayed in Fig. 6 for bins with sample sizes larger than 500. Rainfall intensity at upper quantiles increases exponentially with PW (Fig. 6, first column). The scaling factor, defined as the ***e***-index of the exponential fit to the quantile points, varies among the three sub-regions. For instance, the scaling factors for the 99.9th percentiles are 0.03 (r^2=0.98) in southeastern China, 0.04 (r^2=0.98) in central China, and 0.05 (r^2=0.92) in northwestern China, respectively. This scaling factor also increases with increasing p for precipitation quantiles in all three sub-regions. These results indicate that the intensities of rainfall extremes increase exponentially with available moisture. The sensitivity of this dependence is largest in arid northwestern China and smallest in the humid southeast.

The dependence of rainfall extremes on PW thus can be summarized as

$$\ln P = \alpha PW + c_1$$

where c_1 is a constant and α denotes the efficiency of water vapor being converted to rainfall. This study indicates that α varies from 0.03 to 0.12 for different seasons and sub-regions in China, with the largest values for winter in northwestern China and the smallest values for summer in southeastern China.

3.3 Dependence of precipitation on CAPE

Using the same method, we explore the dependence of precipitation on CAPE by first dividing the daily averages into unevenly spaced bins based on the ten deciles of CAPE values. The mean dependence of precipitation on CAPE is shown in Fig. 5d–f. When compared with the average relationship between precipitation and PW, the relationship between precipitation and CAPE remains generally positive, but with a parabolic structure that hints at saturation (if not reversal) of the relationship at large values of CAPE. The mean rainfall intensity appears to decline for CAPE values exceeding 2000 J kg^{-1} in southeastern China. Similar inflection points can be identified near 800 J kg^{-1} over central China and 600 J kg^{-1} over northwestern China. Although the declines are not statistically significant at the 95% confidence level, this result indicates that larger values of CAPE do not imply larger rainfall amounts; indeed, mean precipitation may decrease with increasing CAPE in certain situations. Note that this relationship may be affected by sampling biases associated with pairing daily precipitation with the average CAPE observed at 00 and 12 UTC (approximately 06~08 and 18~20 local solar time). We discuss this issue further below.

The tendency for precipitation amounts to decline at larger values of CAPE is not statistically significant (Fig. 5d–f); however, indications of signal saturation are robust across all three sub-regions, indicating that the conversion of CAPE into kinetic energy becomes less efficient at larger values of CAPE. This conversion efficiency affects the vertical velocities of convective air parcels, which in turn affect condensation rates and ultimately rainfall intensities. Previous studies suggested that the variation of rainfall quantiles with respect to CAPE may be approximated as $CAPE^{\beta}$ (Lepore *et al.*, 2015). The dependence of rainfall on CAPE can therefore be summarized as

$$\ln P = \beta \ln CAPE + c_2$$

where c_2 is a constant and β denotes the fixed fraction of CAPE converted to upward velocity. Idealized air parcel theory yields a β value of approximately 0.5 (North and Erukhimova, 2009). However, our results indicate values of β between 0.005 and 0.06 for the 99.9th percentile of all rainfall events, with larger values in southeastern China and smaller values in northwestern China (Fig. 6, third column). The quantile curves are nearly parallel to each other in all three sub-regions. When taking seasonal variations into account, β shows a spread that ranges from −0.03 to 0.01, with negative values during summer in all three sub-regions and small positive values during winter in southeastern China. Conditions over China thus diverge considerably from the idealized scenario, in which a large proportion of an increase in CAPE (with all other environmental parameters fixed) translates to an increase in the intensity of the rainfall (Cody *et al.*, 2007). In reality, the proportion of CAPE that is transformed into precipitation is quite small. The weak dependence of rainfall intensities on CAPE is largely due to declines in precipitation in the upper deciles of CAPE, which are particularly pronounced in southeastern China during boreal summer.

The complexity of the dependence of rainfall extremes on CAPE may arise from a combination of several factors, including wind shear, entrainment, and moisture loading, among others (Lepore *et al.*, 2015). For example, conversion efficiency depends on the environmental humidity of the entrained air (Derbyshire *et al.,* 2004), which varies substantially between the southeast and northwest. Some studies have argued that convective inhibition, a measure of the energy barrier inhibiting an air parcel from rising from the surface to the level of free convection, fundamentally undermines the relationship between precipitation and CAPE (Kirkpatrick *et al.*, 2011). When convective inhibition is small, even a modest amount of CAPE can produce updrafts strong enough for precipitation particles to coalesce effectively. Conversely, large values of convective inhibition can be sufficient to suppress the occurrence of updrafts even in the presence of large values of CAPE. The latter situation may contribute to our results indicating a negative relationship between precipitation and CAPE. The occurrence of different types of precipitation may also confound any simple relationship between CAPE and precipitation. Precipitation can occur either due to slow ascent of air in synoptic systems, such as along fronts, or be triggered by local instability and convective motion in the atmosphere. The former type is usually associated with low-intensity precipitation that lasts for several hours to days, while the latter type is associated with stronger precipitation but with a shorter duration. The daily time scale of the data used in this study biases the results toward large-scale precipitation, potentially weakening the implied relationship between precipitation and CAPE (Berg *et al.*, 2009; Haerter and Berg, 2009). Another potential contributing factor is the inability of daily data to represent the phase relationship between CAPE and precipitation (Subrahmanyam *et al.*, 2015). The relevant values of CAPE for a given precipitation event are those preceding the event. As a rough check, we have examined the sensitivity of the results to different permutations of the data, including shifting the CAPE pairs 12 hours earlier (i.e. 12Z at day–1 and 00Z on current day) to better reflect the lead–lag relationship between CAPE and precipitation and examining the daily maximum CAPE rather than the daily mean. The results are qualitatively insensitive to both adjustments.

Relationships of the type reported in this section are essential for identifying appropriate parameter values for convective schemes in contemporary global climate models, most of which rely on CAPE to compute cloud base mass flux (which in turn controls the convective heating and thus the precipitation amount; (e.g., Arakawa and Schubert, 1974). The extent to which the relationships identified in this work hold for convective precipitation specifically, as opposed to all precipitation, would help to determine the extent to which the parameters in these schemes must be adjusted to adequately represent the behavior of convection in these three climate zones in China, and perhaps in similar climate zones worldwide. Careful analysis of high-frequency data collected at representative sites could help to resolve this issue.

3.4 Joint dependence of extreme precipitation on PW and CAPE

To further understand the joint effects of available moisture and atmospheric convection on precipitation, we classify the rainfall events into discrete cells in the PW–CAPE phase space. The joint quantiles of PW and CAPE (shown in Fig. 7) are determined in two steps. First, we bin the daily samples into ten intervals based on the deciles of PW. Second, for samples in each PW bin, we calculate ten decile bins of CAPE using the same approach. This procedure yields in total 100 joint cells with each row/column containing roughly the same number of samples. The grid is defined by the ten decile bins of PW and CAPE used above, thus ensuring approximately equal sample sizes in each column and each row. We then calculate the typical rainfall intensity and the characteristic frequency of rainfall occurrence within each cell (Fig. 7). The frequency of rainfall occurrence is defined as the ratio of rainy days (daily rainfall larger than 0.1 mm) to the total sample sizes within each cell, and for each cell rainfall intensity is calculated by averaging all the rainy events.

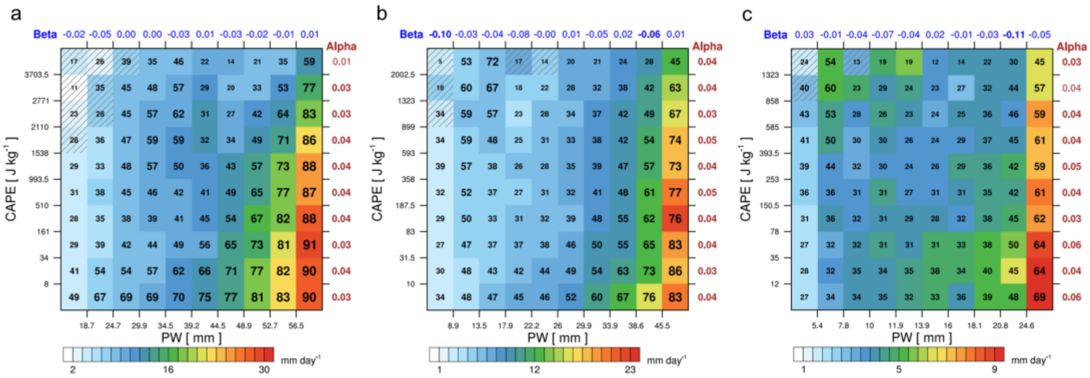

Figure 7. Joint dependence of precipitation on PW and CAPE over (a) southeastern China, (b) central China, and (c) northwestern China. Bold numbers in each cell indicate the frequency of rainfall occurrence, defined as the ratio of rainy days (daily rainfall larger than 0.1 mm) to the total samples in each cell. Larger font sizes indicate higher occurrence frequencies. Color shading denotes rainfall intensity averaged over all rainy days in each cell. The fit coefficients α and β (see text) for the 99.9th rainfall percentile along each row and column are listed along the top and right axes of each panel. Numbers in bold indicate the fit is significant at 95% confidence level. Detailed information for the fit coefficients is listed in Table 1. Hatching indicates cells with sample sizes less than 100, which are excluded from the fitting. Note the different (and irregular) scales for each pair of axes.

Generally, for each CAPE bin, rainfall intensity increases with increasing PW in all three sub-regions. Rainfall maxima consistently occur in the uppermost decile of PW. Although the bulk of precipitation events manifest as light precipitation when PW is relatively small, the frequency of rainfall occurrence within each cell is largely consistent with the distribution of rainfall intensity. Within each PW bin, the relationship between rainfall intensity and CAPE is curvilinear (Fig. 7). More specifically, precipitation and CAPE are positively correlated up to an "optimal" value, and then become negatively correlated with precipitation decreasing as CAPE continues to increase. Overall, the most intense rainfall and the highest frequencies of rainfall occurrence are typically associated with large values of PW but small-to-moderate values of CAPE.

Based on the relationships identified above, we expect the joint dependence of precipitation on PW and CAPE to take the following form:

$$\ln P = \alpha PW + \beta \ln CAPE + c$$

Here, c is a constant, α denotes the efficiency of water vapor conversion to rainfall, and β denotes the fraction of CAPE converted to upward velocity. Among the three sub-regions, smaller values of α correspond to larger values of β in southeastern China, while larger values of α correspond to smaller values of β in northwestern China (Fig. 6). We further examine the dependence of extreme precipitation on PW conditional on percentiles of CAPE and vice versa (Fig. 7 and Table 1). These conditional fits yield similar results to those shown in Fig. 6. Our results therefore imply that the efficiency of water vapor conversion to rainfall and the efficiency of CAPE conversion to upward velocity are geographically complementary within mainland China. We emphasize, however, that moisture availability (rather than CAPE) is the primary limiting factor on both rainfall intensity and the occurrence of rainfall extremes throughout China.

Table 1. Detailed information of conditional fit coefficients (±S.E.) for three different rainfall percentiles (*p*=0.95, 0.99, and 0.999) over three sub-regions based on Fig. 7. For each rainfall percentile, fit coefficients are sorted in ascending order of PW/CAPE quantiles.

	Southeastern China		Central China		Northwestern China	
p	α	β	α	β	α	β
95	**0.04±0.001**	-0.00±0.014	**0.04±0.002**	-0.02±0.010	**0.05±0.005**	**0.05±0.018**
	0.04±0.002	-0.02±0.015	**0.04±0.003**	**0.04±0.013**	**0.05±0.006**	**0.06±0.015**
	0.04±0.002	0.01±0.009	**0.04±0.003**	-0.01±0.006	**0.04±0.007**	-0.01±0.024
	0.04±0.003	-0.00±0.016	**0.04±0.003**	**-0.06±0.013**	**0.04±0.006**	-0.01±0.022
	0.03±0.003	-0.02±0.016	**0.04±0.002**	**-0.05±0.014**	**0.04±0.008**	0.00±0.019
	0.04±0.003	-0.01±0.010	**0.04±0.003**	**-0.02±0.009**	**0.04±0.005**	**-0.09±0.021**
	0.03±0.004	**-0.05±0.014**	**0.04±0.002**	**-0.07±0.011**	**0.03±0.008**	-0.06±0.035
	0.02±0.004	**-0.08±0.024**	**0.03±0.003**	**-0.04±0.010**	**0.03±0.009**	-0.03±0.017
	0.01±0.003	**-0.10±0.021**	**0.03±0.003**	**-0.05±0.014**	0.01±0.014	**-0.10±0.021**
	0.02±0.006	**-0.07±0.028**	**0.03±0.003**	-0.04±0.021	0.01±0.009	**-0.06±0.010**
99	**0.03±0.002**	0.00±0.016	**0.04±0.003**	-0.05±0.021	**0.05±0.005**	0.01±0.034
	0.04±0.002	-0.01±0.024	**0.04±0.003**	-0.00±0.012	**0.05±0.003**	0.04±0.020
	0.04±0.002	0.02±0.020	**0.04±0.003**	-0.03±0.021	**0.05±0.006**	-0.01±0.021
	0.04±0.003	0.00±0.011	**0.04±0.002**	**-0.09±0.026**	**0.04±0.008**	-0.04±0.022
	0.03±0.002	-0.03±0.016	**0.04±0.003**	-0.06±0.030	**0.04±0.005**	-0.03±0.021
	0.03±0.002	0.00±0.017	**0.04±0.002**	**-0.03±0.012**	**0.05±0.007**	**-0.05±0.012**
	0.03±0.006	**-0.04±0.015**	**0.04±0.003**	**-0.04±0.012**	**0.04±0.006**	-0.05±0.047
	0.02±0.004	-0.04±0.027	**0.04±0.003**	-0.02±0.016	**0.04±0.010**	-0.05±0.034
	0.02±0.004	**-0.06±0.025**	**0.04±0.005**	**-0.04±0.006**	0.03±0.013	-0.06±0.029
	0.02±0.006	-0.04±0.024	**0.03±0.003**	-0.03±0.019	**0.03±0.010**	**-0.06±0.017**
99.9	**0.03±0.005**	-0.02±0.014	**0.04±0.003**	**-0.10±0.026**	**0.06±0.007**	0.03±0.043
	0.04±0.003	-0.05±0.027	**0.03±0.004**	-0.03±0.020	**0.04±0.013**	-0.01±0.044
	0.03±0.004	0.00±0.024	**0.04±0.005**	-0.04±0.021	**0.06±0.007**	-0.04±0.035
	0.04±0.003	0.00±0.016	**0.04±0.003**	-0.08±0.063	**0.03±0.010**	-0.07±0.045
	0.04±0.004	-0.03±0.019	**0.05±0.007**	-0.00±0.066	**0.04±0.008**	-0.04±0.049
	0.04±0.005	0.01±0.031	**0.04±0.008**	0.01±0.019	**0.05±0.010**	0.02±0.060
	0.04±0.006	-0.03±0.020	**0.05±0.004**	-0.05±0.027	**0.04±0.010**	-0.01±0.049
	0.03±0.005	-0.02±0.035	**0.03±0.004**	0.02±0.021	**0.04±0.013**	-0.03±0.049
	0.03±0.003	-0.01±0.023	**0.04±0.007**	**-0.06±0.023**	0.04±0.022	**-0.11±0.037**
	0.01±0.009	0.01±0.036	**0.04±0.004**	0.01±0.030	**0.03±0.011**	-0.05±0.032

Note: numbers in bold indicate the fit is significant at 95% confidence level

4 Summary and discussion

This study builds on previous research regarding the influence of atmospheric temperature on precipitation intensities by exploring two key mechanisms by which these influences can be expressed: available water vapor and convective instability. We represent these two mechanisms by PW and CAPE, respectively, and examine how rainfall intensities, and especially rainfall extremes, depend on PW and CAPE within mainland China. Through this work, we intend to stimulate additional ideas and research targeting the influence of temperature on rainfall intensity. Our main findings can be summarized as follows.

1. To our knowledge, we present the first comprehensive evaluation of the spatial distributions and seasonal cycles of PW and CAPE over the mainland China based on radiosonde station observations. Dividing the 144 stations into three sub-regions (southeastern China, central China, and northwestern China), we find that precipitation, PW, and CAPE consistently decrease across China from the southeast to the northwest. All three variables follow well-defined seasonal cycles, with maximum values during boreal summer and minimum values during winter.
2. Rainfall and PW are positively correlated, with rainfall extremes increasing exponentially with PW (i.e., $\ln(P) \sim \alpha \cdot \mathrm{PW}$). The parameter α varies by season and location, and represents the efficiency with which available water vapor is converted to rainfall. This efficiency is higher in northwestern China, where water vapor is scarce, than in southeastern China, where water vapor is plentiful.
3. We find a power law relationship between rainfall intensity and CAPE (i.e., $\ln(P) \sim \beta \cdot \ln(\mathrm{CAPE})$. The parameter β also varies by location and seasons, with indications that it may be negative during boreal summer. This result indicates that the fraction of CAPE converted to upward velocity is much less than that implied by idealized calculations. This difference can be attributed to a variety of environmental factors, as discussed in section 3.3. In contrast to the conversion of water vapor to rainfall, the conversion of CAPE to upward motion is more efficient in the humid southeast than it is in the arid northwest.
4. The joint dependence of precipitation on PW and CAPE can thus be summarized in the form $\ln(P) \sim \alpha \cdot \mathrm{PW}+\beta \cdot \ln(\mathrm{CAPE})$. Our results indicate that the geographical values of α and β are complementary among the three sub-regions: a lower efficiency of water vapor conversion to rainfall corresponds to a larger fraction of CAPE converted to upward velocity in southeastern China, while a smaller fraction of CAPE converted to upward velocity corresponds to a higher efficiency of water vapor conversion to rainfall in northwestern China. However, rainfall intensity, and especially the intensity of rainfall extremes, is predominantly controlled by variations in water vapor availability (PW) in all three sub-regions, with the intensity of convection (CAPE) playing a secondary role.

The findings presented in this work provide a useful starting point for further research on this topic, but several important questions remain unanswered. For example, the causes for the weak dependence of rainfall intensities on CAPE found in this work are unclear. We have proposed several factors that may contribute to this weak dependence, but distinguishing among these possibilities will require data with improved precision and temporal sampling. Data sets that can better distinguish the type, duration, and diurnal cycles of rainfall and its co-variations with PW and CAPE will be necessary to resolve this issue. Reanalysis products can provide estimates of

CAPE at higher spatial and temporal resolution, and represent a potentially viable alternative data source for this type of study (cf. Lepore et al. 2015). However, we argue that these reanalysis-based estimates should be used with caution. For example, although the ERA-Interim reanalysis assimilates a variety of qualitychecked observations, the CAPE products are calculated from forecast fields (i.e. prior to the data assimilation step; Dee et al. 2011). In addition, despite the increased coverage, reanalysis-based estimates of CAPE are not necessarily more representative than the radiosonde-based estimates we have used in this study. Again using ERA-Interim as an example, we find that the reanalysis CAPE product substantially underestimates our observationally-based estimates (Fig. 8), especially in northwestern China where the topography is complex. This result is consistent with the conclusions of Taszarek et al. (2018), who compared 1 million sounding based measurements of CAPE with estimates from ERA-Interim in Europe. They found that the reanalysis products were largely unable to capture the observed variations, and suggested that this may arise from deficiencies in boundary layer representations. A detailed intercomparison between radiosonde and reanalysis-based estimates would undoubtedly be instructive, but would need to carefully account for differences in definitions and calculation methods, and is beyond the scope of this study. Intense rainfall associated with typhoons may confound the deduced dependence of rainfall intensities on CAPE, particularly along the southeastern coast of China. Here we briefly investigate the potential sensitivity of our results to the impacts of typhoons. We divide the observed rainfall events in southeastern China into two groups based on whether they are 'affected' or 'unaffected' by typhoon events. Given that the average typhoon size in the western North Pacific is about 200 km (Lu et al. 2011; Chan and Chan 2012), a rainfall event is labelled as 'affected' if a typhoon was active within 200 km of the station where the observations were collected. Based on this criterion, there are a total of 3794 time steps that qualify as 'affected' during 1961–2015. However, these time steps comprise only 518 rainfall events (when both CAPE values and rainfall records are available), against 14,105 rainfall events that were not affected by a typhoon. The dependence of rainfall intensities on CAPE with and without typhoon effects are shown in Fig. 9. The mean dependence of precipitation events affected by typhoons (Fig. 9a) shows a general decrease in precipitation intensity as CAPE increases. By contrast, the dependence of precipitation intensity on CAPE during 'unaffected' events is similar to that shown in Fig. 5d, with a generally positive relationship but hints of a decline at larger values of CAPE (Fig. 9b). This is also consistent with the third column in Fig. 6, in which the curves for different rainfall percentiles are nearly parallel to each other, indicating that the relationships are robust across a large range of rainfall intensities. Although not statistically significant, these results suggest that rainfall events affected by typhoons have a quite different relationship with CAPE. However, the potential influences of typhoons concern less than 3% of the total sample size, and have no meaningful impact on the results.

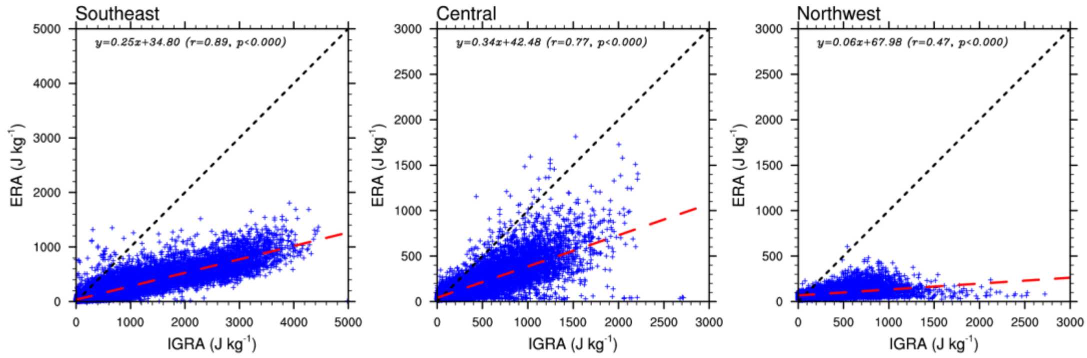

Figure 8. Scatter plots of daily CAPE values using ERA-Interim forecast products (y-axis) and radiosonde observations (x-axis) during 1979–2015 for the three sub-regions. Red dashed lines show least-squares linear fits, with equations as listed along the inside of the top axis in each panel.

Finally, we emphasize the complementary geographic variations between the efficiency of water vapor conversion to rainfall and the fraction of CAPE converted to upward velocity are not yet well understood. Numerical simulations will be needed to better understand the reasons for these geographically distinct sensitivities of rainfall intensity to atmospheric temperature among different climate zones in mainland China. Research along these lines will be important for evaluating and improving the reliability of climate projections in China and beyond.

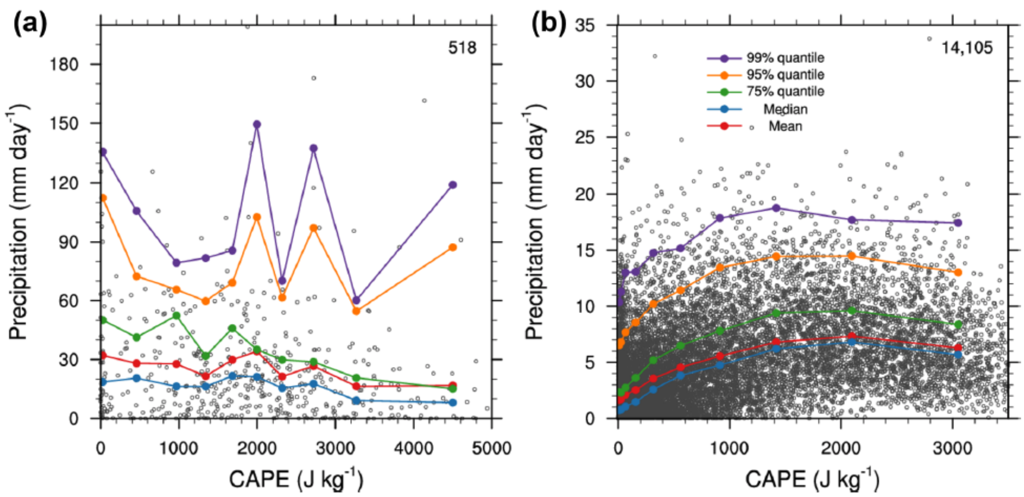

Figure 9. The mean dependence of precipitation intensity on CAPE for precipitation events that are a affected and b unaffected by typhoons in southeastern China (see text for details). Dots represent available events within each category. The number of samples is listed at the top right corner of each panel. Note the different axis scales between the two panels.

Acknowledgments and Data

We gratefully acknowledge NOAA National Centers for Environment Information for providing public access to the IGRA radiosonde data (doi:10.7289/V5X63K0Q), which are available at https://www.ncdc.noaa.gov/data-access/weather-balloon/integrated-global-radiosonde-archive. We would like to thank National Meteorological Information Center of Chinese Meteorological Administration for providing daily gauge-based precipitation data (http://data.cma.cn/en). This work was supported by the Ministry of Science and Technology of China (2014CB441303).

References

1. Berg, P. and coauthors (2009), Seasonal characteristics of the relationship between daily precipitation intensity and surface temperature, *J. Geophys. Res.*, 114, D18102, doi:10.1029/2009JD012008.
2. Brooks, H. E., G. W. Carbin and P. T. Marsh (2014), Increased variability of tornado occurrence in the United States, *Science*, 346, 349-352.
3. Brooks, H. (1994), On the environments of tornadic and nontornadic mesocyclones, *Weather ad Forecasting*, 9, 606-618.
4. Chen, G. T.-J. (1994), Large-scale circulations associated with the East Asian summer monsoon and the Mei-Yu over South China and Taiwan, *J. Meteorol. Soc. Jpn.*, 72, 959–983.
5. Kirkpatrick, C., E. W. McCaul, and C. Cohen, (2011), Sensitivities of simulated convective storms to environmental CAPE. *Mon. Wea. Rev.*, 139, 3514–3532.
6. Dee, D. P., *et al.* (2011), The ERA-Interim reanalysis: Configuration and performance of the data assimilation system, *Q. J. R. Meteorol. Soc.*, 137(656), 553–597.
7. DeMott, C. A., and D. A. Randall (2004), Observed variations of tropical convective available potential energy, *J. Geophys. Res.*, 109, D02102.
8. Derbyshire, S. H., I. Beau, P. Bechtold, J. –Y. Grandpeix, J. –M. Piriou, J. –L. Redelsperger and P. Soares (2004), Sensitivity of moist convection to environmental humidity, *Q. J. R. Meteorol. Soc.*, 130, 3055–3079.
9. Donat, M., A. L. Lowry, L. V. Alexander, P. A. O'Gorman and N. Maher (2016), More extreme precipitation in the world's dry and wet regions, *Nature Clim. Change*, 6, 508-513.
10. Donner, L. J. & V. T. Phillips (2003), Boundary layer control on convective available potential energy: Implications for cumulus parameterization. *J. Geophys. Res.*, 108(D22), 4701.
11. Doswell, C. A., III, and E. N. Rasmussen, The effect of neglecting the virtual temperature correction on CAPE calculations, *Weather Forecast.*, 9, 625–629, 1994.
12. Durre, I., R. S. Vose, and D. B. Wuertz (2006), Overview of the Integrated Global Radiosonde Archive, *J. Clim.*, 19, 53–68.
13. Durre, I., Williams, C. N., Yin, X., & Vose, R. S. (2009). Radiosonde-based trends in precipitable water over the Northern Hemisphere: An update. *J. Geophys. Res.: Atmospheres*, 114(D5).
14. Emanuel, K. A., *Atmospheric Convection*, 580 pp., Oxford Univ. Press, New York, 1994.
15. Gordon, N. D., A. K. Jonko, P. M. Forster, and K. M. Shell (2013), An observationally based constraint on the water-vapor feedback, *J. Geophys. Res.*

Atmos., 118, 12435-12443.

16. Haerter, J. O., and P. Berg (2009), Unexpected rise in extreme precipitation caused by a shift in rain type?, *Nat. Geosci.*, 2,372–373, doi:10.1038/ngeo523.
17. Hettmansperger, T. P., and S. J Sheather (1986), Confidence Intervals Based on Interpolated Order Statistics. *Statistics and Probability Letters* 4, 75–79. doi:10.1016/0167-7152(86)90021-0.
18. Kunkel, K. E., T. R. Karl, D. R. Easterling, K. Redmond, J. Young, X. Yin, and P. Hennon (2013), Probable maximum precipitation and climate change, *Geophys. Res. Lett.*, 40, 1402–1408.
19. Lenderink, G., and E. van Meijgaard (2008), Increase in hourly precipitation extremes beyond expectations from temperature changes, *Nat. Geosci.*, 1, 511–514, doi:10.1038/ngeo262.
20. Lepore, C., D. Veneziano, and A. Molini (2015), Temperature and CAPE dependence of rainfall extremes in the eastern United States, *Geophys. Res. Lett.*, 42, 74–83, doi:10.1002/2014GL062247.
21. Lu, E. *et al.* (2014). Changes of summer precipitation in China: The dominance of frequency and intensity and linkage with changes in moisture and air temperature. *J. Geophys. Res. Atmos.*, 119(12), 575–512, 587, doi: 10.1002/2014jd022456.
22. North, G. R., and T. L. Erukhimova (2009), *Atmospheric Thermodynamics*, Cambridge Univ. Press, New York.
23. Nyblom, J. (1992), Note on Interpolated Order Statistics. S*tatistics and Probability Letters*. 14, 129–31. 10.1016/0167-7152(92)90076-H.
24. O'Gorman, P. A., and T. Schneider (2009), The physical basis for increases in precipitation extremes in simulations of 21st century climate change, *Proc. Natl. Acad. Sci. U. S. A.*, 106(35), 14,773–14,777, doi:10.1073/pnas.0907610106.
25. Singh, M. and O'Gorman, P (2013), Influence of entrainment on the thermal stratification in simulations of radiative-convective equilibrium, *Geophys. Res. Lett.*, 41, 6037–6044.
26. Subrahmanyam, K., K. Kumar, A. Babu (2015), Phase relation between CAPE and precipitation at diurnal scales over the Indian summer monsoon region. *Atmos. Sci. Lett.*, 16, 346–354.
27. Trapp, R. J., N. S. Diffenbaugh, H. E. Brooks, M. E. Baldwin, E. D. Robinson, and J. S. Pal (2007), Changes in severe thunderstorm environment frequency during the 21st century caused by anthropogenically enhanced global warming radiative forcing, *Proc Natl Acad Sci USA*, 104, 19719–19723.
28. Trenberth, K. E. (1998), Atmospheric moisture residence times and cycling: Implications for rainfall rates and climate change, *Clim. Change*, 39, 667–694.
29. Trenberth, K. E., and D. J. Shea (2005), Relationships between precipitation and surface temperatures, *Geophys. Res. Lett.*, 32, L14703.
30. Trenberth, K. E. (2011), Changes in precipitation with climate change. *Clim. Res.*, 47, 123–138.
31. Utsumi, N., S. Seto, S. Kanae, E. E. Maeda, and T. Oki (2011), Does higher surface temperature intensify extreme precipitation?,*Geophys. Res. Lett.*, 38, L16708, GL048426.

32. Wang, Y., and L. Zhou (2005), Observed trends in extreme precipitation events in China during 1961–2001 and the associated changes in large-scale circulation, *Geophys. Res. Lett.*, 32, L09707.
33. Ye, H. and coauthors (2014), Impact of increased water vapor on precipitation efficiency over northern Eurasia, *Geophys. Res. Lett.*, 41, 2941–2947, doi:10.1002/2014GL059830.
34. Yuan, Z. *et al.* (2015), Historical changes and future projection of extreme precipitation in China, *Theor. Appl. Climatol*. doi:10.1007/s00704-015-1643-3.
35. Zhou, T. and Z. Li, (2002), Simulation of the East Asian summer monsoon using a variable resolution atmospheric GCM. *Climate Dyn.*, 19, 167–180